Acta Materialia 237 (2022) 118132

Contents lists available at ScienceDirect

Acta Materialia

journal homepage: www.elsevier.com/locate/actamat

Full length article

Theory-guided design of high-strength, high-melting point, ductile, low-density, single-phase BCC high entropy alloys

Y. Rao[a,*], C. Baruffi[a], A. De Luca[b], C. Leinenbach[b,c], W.A. Curtin[a]

[a] Laboratory for Multiscale Mechanics Modeling, École Polytechnique Fédérale de Lausanne, 1015 Lausanne, Switzerland
[b] Empa, Swiss Federal Laboratories for Materials Science and Technology, Überlandstrasse 129, CH-8600 Dübendorf, Switzerland
[c] Laboratory for Photonics Materials and Characterization, Ecole Polytechnique Fédérale de Lausanne, 1015 Lausanne, Switzerland

ARTICLE INFO

Article history:
Received 14 March 2022
Revised 7 June 2022
Accepted 27 June 2022
Available online 7 July 2022

ABSTRACT

The search for new high-temperature alloys that can enable higher-efficiency/lower-emissions power generation has accelerated with the discovery of body-centered cubic (bcc) refractory High Entropy Alloys (HEAs). These many-component, non-dilute alloys in the Cr-Mo-W-V-Nb-Ta-Ti-Zr-Hf-Al family hold the potential for combining high strength and thermodynamic stability at high temperature with low density and room-temperature ductility, but searching the immense compositional space is daunting. Here, very recent theories and expanded thermodynamic tools are used to guide the discovery of new alloys satisfying the required suite of properties. The search and discovery method is first demonstrated for 5-component equicomposition alloys, identifying HfMoNbTaTi as the one alloy satisfying many constraints, with predicted properties agreeing with experiments. The design process then discovers new quinary and quarternary alloys in the Hf-Mo-Nb-Ta-Ti space having even better overall properties. One new quinary alloy is fabricated and shown to be single phase with high room temperature hardness, high melting point, and low density. More broadly, the new design process can further be used to explore millions of alloys with other desired multi-dimensional performance requirements.

1. Introduction

High Entropy Alloys (HEAs) are a new class of essentially random solid solution alloys containing five or more elements in near-equal concentrations [1,2]. For a 5-component alloy selected from among 10 possible elements, there are over 10 million different alloys at composition increments of 5%. Somewhere in that vast space may lurk the few alloys that will satisfy multiple application requirements, such as strength, ductility, thermodynamic stability, and oxidation resistance. To date, only a tiny fraction of the space of either FCC alloys in the Co-Cr-Fe-Mn-Ni-V+ family or BCC alloys in the Cr-Mo-W-V-Nb-Ta-Ti-Hf-Zr-Al family have been fabricated, characterized, and tested. The cost of exploring the entire phase space with only historical data and intuitive knowledge is inaccessibly high. Database and machine learning methods [3–8] hold promise but the amount of data available is paltry compared to the typical scales on which machine learning is applied in other domains. Finding new high-performance alloys must thus rely on a *physics – based* understanding of the connection between properties and composition. That is, screening across millions of alloys is best done using validated mechanistic theories that can be simplified to accurate but easily-computable forms.

With this perspective, we apply recent theoretical models along with thermodynamic assessment to discover new refractory BCC alloys that have high strength, high strength retention at high temperature, surrogate properties indicating possibly sufficient ductility at room temperature, moderate density, high melting temperature, and low single-phase decomposition temperature; these properties constitute the major requirements for critical applications of this class of alloys. In this study, we first report a set of equicomposition alloys that satisfy realistic challenging requirements. Several alloys have already been studied experimentally, enabling validation of our approach. We then identify new non-equicomposition alloys that are predicted to be even more promising. We have fabricated, characterized and tested one of the selected alloys, further confirming this alloy selection strategy. The method is general, and can be adapted to other performance requirements.

* Corresponding author.
E-mail address: you.rao@epfl.ch (Y. Rao).

https://doi.org/10.1016/j.actamat.2022.118132

2. Theories for the design process

The room temperature yield strength is evaluated using a fully-analytic parameter-free model for edge dislocation strengthening in BCC HEAs [9,10]. Edge dislocations are more likely to retain strength at high temperatures because (i) a vacancy mechanism defeats screw strengthening at high homologous (T/T_m) temperatures [11,12] and (ii) the input parameters to the edge theory can be reasonably estimated, unlike those for screw theories. In an N-component alloy at composition $\{c_n\}$ $(n = 1, 2, \ldots, N)$, edge strengthening is dominated by the interactions between the solute misfit volumes $\{\Delta V_n\}$ in the alloy and the pressure field generated by the edge dislocation of Burgers vector b, which scales with the alloy elastic constants $\overline{\mu}$ and $\overline{\nu}$. The analytic model for yield strength reduces to equations for the zero temperature strength and the zero temperature energy barrier of

$$\tau_{y0} = 0.040\alpha^{-1/3}\bar{\mu}\left(\frac{1+\bar{\nu}}{1-\bar{\nu}}\right)^{4/3}\left[\frac{\sum_n c_n \Delta V_n^2}{\bar{b}^6}\right]^{2/3} \tag{1}$$

$$\Delta E_b = 2.00\alpha^{1/3}\bar{\mu}\bar{b}^3\left(\frac{1+\bar{\nu}}{1-\bar{\nu}}\right)^{2/3}\left[\frac{\sum_n c_n \Delta V_n^2}{\bar{b}^6}\right]^{1/3} \tag{2}$$

leading to the finite-T, finite strain rate $\dot{\epsilon}$ yield stress that can be well-described over a wide temperature range by the ad-hoc form

$$\tau_y(T, \dot{\epsilon}) = \tau_{y0}\exp\left[-\frac{1}{0.55}\left(\frac{k_B T}{\Delta E_b \ln\left(\frac{\dot{\epsilon}_0}{\dot{\epsilon}}\right)}\right)^{0.91}\right] \tag{3}$$

where $\dot{\epsilon_0} = 10^4\ s^{-1}$ is a reference strain rate and $\alpha = 1/12$ is a line-tension coefficient. To create a fast efficient model, the elemental misfit volumes ΔV^n and alloy elastic constants $\bar{C}_{ij}$ are estimated using Vegard's Law [10]

$$\overline{C}_{ij} = \sum_{n=1}^{N} c_n C_{ij}^n; \quad \overline{V} = \sum_{n=1}^{N} c_n V_n; \quad \Delta V_n = V_n - \overline{V} \tag{4}$$

$$\overline{\mu} = \sqrt{\frac{1}{2}\overline{C}_{44}(\overline{C}_{11} - \overline{C}_{12})}; \quad \overline{B} = (\overline{C}_{11} + 2\overline{C}_{12}); \quad \overline{\nu} = \frac{3\overline{B} - 2\overline{\mu}}{2(3\overline{B} + \overline{\mu})} \tag{5}$$

with the $\bar{\mu}$ and $\bar{\nu}$ calculated using the Bacon-Scattergood relationships [13–15].

The ductility of BCC HEAs has been related to the *intrinsic* fracture behavior at a sharp crack tip [16–18]. The intrinsic ductility is tied mainly to the ratio between the fracture surface energy γ_s and the unstable stacking fault energy γ_{usf} of the relevant dislocation slip plane emanating from a crack tip. To circumvent the computational bottleneck of extremely expensive first-principles calculations, it has been proposed that the intrinsic ductility scales with the alloy Valence Electron Count, $\overline{\text{VEC}} = \sum c_n \text{VEC}_n$, where VEC_n is the VEC for element n in the alloy (Ti,Hf,Zr=4; V,Nb,Ta=5; Cr,Mo,W=6) [16,18,19]. Mak et al. [18] found that VEC = 5.0 is an approximate borderline, with more-ductile materials having VEC < 5.0.

The thermodynamic properties are assessed using the CalPhaD software ThermoCalc with the newest TCHEA5 database. This database includes information on 310 binary and 493 ternary alloys of 26 elements including the refractory elements of interest here. Most binary systems have been evaluated for full temperature and composition ranges while 192 of the ternaries have been critically assessed. Studies on some BCC HEAs using earlier generations of the TCHEA databases have shown some success versus experiments [20], providing enhanced confidence for the use of the more-complete database. For each alloy of interest, we calculate the equilibrium phases and their molar fractions versus temperature and then extract the melting point T_m and the temperature T^* below which the single-composition random phase decomposes into sub-phases. A desirable alloy should have a a high T_m and a low T^* such that it can be fabricated and used in a wide single phase domain.

3. Alloy design with constraints: Results

Our design process first sets a target room temperature yield strength and alloy VEC. Candidates satisfying these criteria are then examined for single-phase thermodynamic stability and high melting point needed for high-temperature strength retention. We consider quinary HEAs formed from the 8-component (alphabetically ordered) family Cr-Hf-Mo-Nb-Ta-Ti-W-Zr. We eliminate *a priori* both Al, due to its strong tendency for intermetallic formation [21–24] and V, due to its low oxide melting temperature (≈ 675 °C) [25,26].

To first validate our theory-guided alloy design procedure, we focus on equicomposition quinary alloys with performance requirements $\tau_y > 1.4$ GPa at $T = 298K$ and $\dot{\epsilon} = 10^{-3}\ s^{-1}$ and VEC < 5.0. From 56 possible equicomposition quinary alloy candidates, 18 satisfy the mechanical criteria. Thermodynamic studies then show that 12 alloys show no single phase domain (Fig. A.1). These alloys generally contain Cr or a combination of W and Zr, and form Laves and/or HCP phases. This is unfortunate, since Cr is the smallest element, Zr the largest, and W the stiffest, and hence single-phase alloys with Cr, Zr, and/or W would tend to have high strengths. Five alloys have only a narrow single phase domain with fairly high decomposition temperatures (Fig. A.2). The one remaining alloy HfMoNbTaTi has excellent properties (Fig. 1). In particular, it has a predicted melting point of 2145 °C, a decomposition temperature of only 854 °C, a predicted room temperature yield strength of 1.48 GPa, and a VEC = 4.8. Detailed data on all six single-phase alloys are listed in Table B.1.

The HfMoNbTaTi alloy identified by our methodology has been studied experimentally [27]. As-cast HfMoNbTaTi is single phase with room temperature yield strength at $10^{-3}\ s^{-1}$ greater than 1.3 GPa, a compressive failure strain greater than 25% (Fig. 1(b)), and high strength retention at high T (700 MPa at 1200 °C, 367 MPa at 1400 °C) consistent with a high T_m. All these results are consistent with our predictions. The experiments also show the well-established plateau in strength at intermediate temperatures that is absent from the theory but always enhancing strengths above the predicted values. The origins of this plateau are a subject of current study, with one possible mechanism being dynamic strain aging (DSA) since the plateau implies zero strain rate sensitivity that can be achieved by DSA. The other identified alloys with narrow single-phase domains have also been studied experimentally in the as-cast condition. The room temperature compressive stress strain curves are shown in Fig. 2(a) and the high temperature strengths are shown in Fig. 2(b) together with our predictions. Some of these alloys have low ductility, but the true ductility might be compromised by, for instance, high interstitial O, N, or C content (precise value not reported) and/or lack of homogenization, all of which are outside the VEC correlation, are not predictable, and must be solved by processing refinements. Despite the higher strengths these alloys exhibit at lower temperatures, HfMoNbTaTi possesses the highest strengths at elevated temperatures, consistent with its having the highest melting point among these alloys, the widest single-phase range, and the best ductility. HfMoNbTaTi thus has the best overall properties, consistent with our predictions. With no experimental inputs, our theory-guided alloy design process has identified the most at-

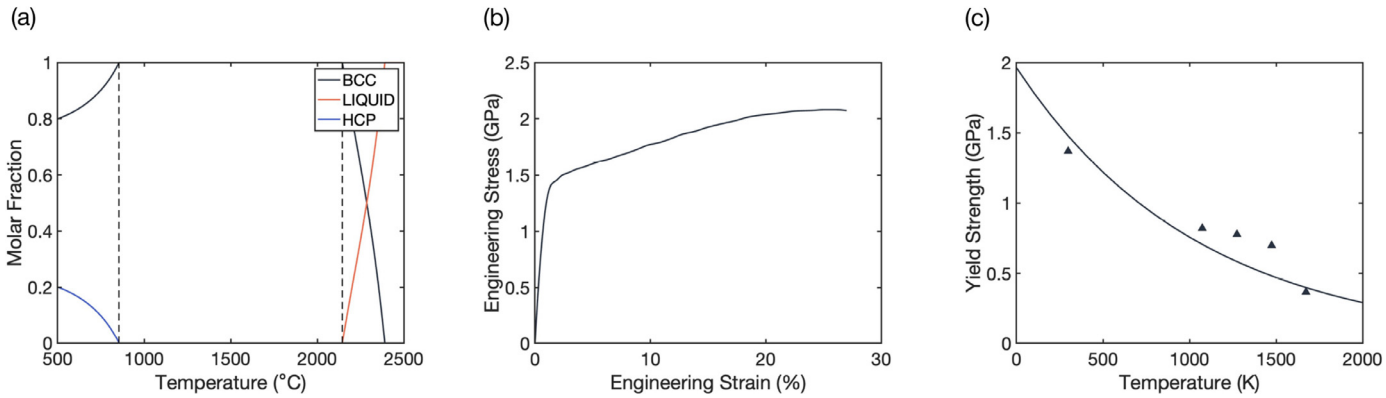

Fig. 1. Properties of the selected alloy HfMoNbTaTi. (a) Molar fraction of stable phases as a function of temperature. The notations BCC represents a BCC random solid solution while HCP is a random HCP phase; (b) Compressive stress-strain curve at room temperature and (c) predicted yield strength τ_y versus temperature T (solid lines) in comparison with experiment results (markers). The experimental data are from Tseng et al. [27].

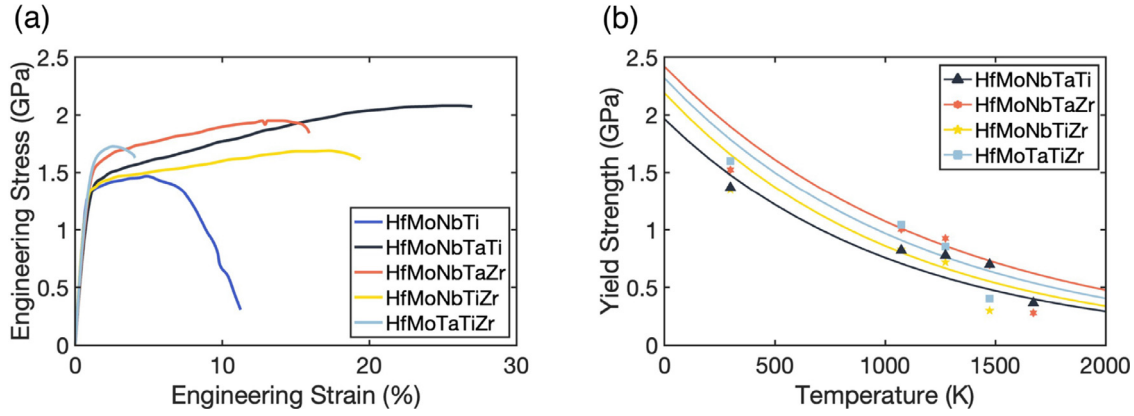

Fig. 2. (a) Compressive stress-strain curve at room temperature and (b) predicted yield strength τ_y versus temperature T (solid lines) in comparison with experiment results (markers) for the equiatomic single phase quinary high entropy alloys. The experimental data are from [27,28].

tractive quinary equicomposition alloy according to our design constraints.

There is no restriction of our design strategy to equicomposition alloys. We thus proceed to find alloys that better satisfy a range of application criteria. The design framework immediately identifies property trade-offs. A lower VEC requires less Mo, but Mo provides considerable strengthening due to its smaller size and higher stiffness. A lower density requires less Hf, but Hf is the largest-size element and confers high strength. “Optimal” is thus associated with specific practical needs and constraints. To expand the composition domain, we sacrifice strength in exchange for lower density, lower VEC (likely more-ductile) alloys that retain a high melting point (and hence high-T strength). These goals are achieved by starting with the very attractive HfMoNbTaTi alloy and executing our design strategy for the Hf-Mo-Nb-Ta-Ti family. We aim then to discovery new quinary alloys with strength > 1.1 GPa, density $\rho < 9$ g/cm^3, VEC < 4.8, and melting temperature $T_m > 2000$ °C within the elemental composition range of 5% - 40% for each element. From 2634 candidate alloys, only 13 satisfy the mechanical property criteria and 10 have $T_m > 2000$°C, all with a wide single phase domain. The key properties of these alloys are shown in Fig. 3 with respect to the equiatomic HfMoNbTaTi (see detailed data in Table B.2). With both lower strength and lower density, the specific strength (strength/density) are nearly unchanged. The alloy $Hf_{15}Mo_{25}Nb_{20}Ta_5Ti_{35}$ is notable, having a lower VEC, lower density, higher specific strength, and comparable melting temperature as compared to HfMoNbTaTi. A second attractive alloy is $Hf_{15}Mo_{35}Nb_5Ta_5Ti_{40}$, with slightly lower melting temperature (2004°C) but lower density and higher strength than HfMoNbTaTi. These results demonstrate the capability of our theory-guided selection procedure to identify promising compositions based on property trade-offs with no further input.

4. Preliminary experimental validation

A sample with the nominal composition $Hf_{15}Mo_{25}Nb_{20}Ta_5Ti_{35}$ identified by our design process was arc-melted using 99.95 + % pure metals in slugs, foil or wire shapes. The button, weighing 10 g, was melted on a water-cooled copper hearth using an Amazemet Repowder 2 system, and flipped ten times to improve homogeneity. The material was sliced using a diamond blade to reveal vertical sections.

Samples for microstructural investigations were cold mounted in epoxy, ground, and polished down to 1 μm diamond suspension. The final polishing was done with 50 nm colloidal silica. Optical microscopy was conducted on a Leica VZ700C optical microscope. Scanning electron microscopy (SEM) was conducted at 30 keV on an FEI Quanta 650 FEG ESEM in backscatter mode (BSE) for Z-contrast imaging. Chemical analysis was performed using an energy-dispersive X-ray spectroscopy (EDX) detector (Thermo Fischer Pathfinder SDD EDX system). The average sample composition was determined by SEM-EDX. Phase identification was performed on an X-ray diffraction (XRD) pattern acquired on a Bruker D8, using the CuKα radiation and a 2 mm diameter pinhole, with a scan between 0 and 100. Rietveld analysis was conducted on the diffraction pattern using a diffraction program (Maud). The microhardness of the alloy was measured with a Fischerscope HM2000

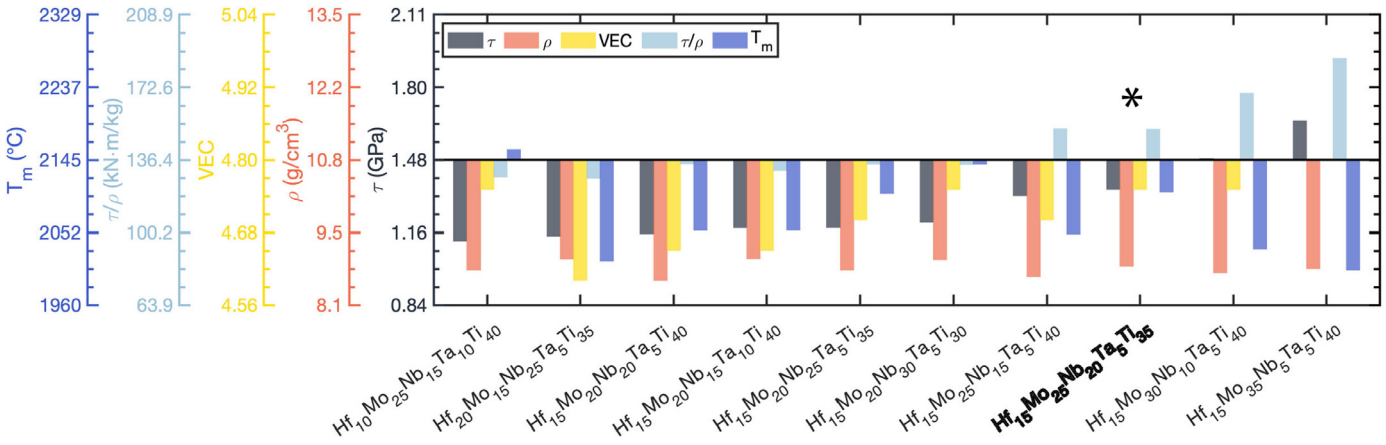

Fig. 3. Key properties of the 10 selected alloys with lower densities with respect to the equiatomic HfMoNbTaTi. The fabricated alloy $Hf_{15}Mo_{25}Nb_{20}Ta_5Ti_{35}$ is highlighted in bold with an asterisk.

hardness tester, with a load of 2 N, for 60 s. The reported microhardness is the average of 15 indents.

To determine the melting point, a sample was heated in an induction furnace equipped with a dual wavelength pyrometer (TYPE) series QKTR 1085 with a range of measurement of 700–2500 °C. The pyrometer was calibrated by measuring the liquidus temperature of commercially pure Ti (T_{liq} = 1670 °C). The sample was placed in an amorphous graphite crucible which was placed in a ZrO_2 crucible filled with corundum (Al_2O_3) sand. The crucibles were then put in the center of a water-cooled Cu induction coil. The surface temperature of the sample was measured continuously with the pyrometer. The temperature was increased manually to a maximum temperature of 2000 °C at a rate of approximately 100 K/min and the sample was observed with a CCD camera. The temperature was not increased further in order to prevent melting of the corundum sand, which starts at approximately 2040 °C.

Selected samples were homogenized in a vacuum furnace at a pressure of $1 - 5 \times 10^{-5}$ mbar. The temperature was increased by 10 K/min, from room temperature to homogenizing temperature at 1363 ± 10°C and held for 1h. Full homogenization typically requires several days, which was not possible in our local system. Due to the high temperature, the sample temperature could not be measured using a thermocouple. Similarly, the cooling rate after solutionizing was not controlled.

The as-cast composition is $Hf_{16}Mo_{23}Nb_{21.3}Ta_{4.5}Ti_{35.2}$ using SEM-EDX. XRD analysis reveals a single BCC phase with average lattice parameter 3.2818 Å. The as-cast material has a dendritic structure (Fig. 4) with evidence of elemental segregation leading to local variations ($\sim \pm 5\%$) of the lattice parameter that suggested Ti and Hf segregation to the interdendritic domains and Mo, Nb and Ta remaining in the dendrites. After the short homogenization treatment, the dendritic structure was still present but the alloy also remained single phase with a low fraction of isolated oxide particles close to entrapped gas porosity. The interstitial contents were measured to be 0.01%C, 0.02%N and 0.08%O, which are quite high and, if maintained in solution, would be expected to reduce ductility substantially and increase strength relative to theory predictions.

Properties of the as-cast alloy are consistent with our predictions. The melting point is confirmed to be > 2000 °C and the density $\rho = 8.86$ g/cm^3 is low. Furthermore, the measured room temperature hardness is 4.96 ± 0.12 GPa (as-cast) and 5.32 ± 0.38 GPa (partially-annealed), corresponding to yield strengths estimated as 1.50 GPa and 1.61 GPa (HV/3.3), respectively. The strengths being higher than predicted may reflect the high interstitial content. Strength predictions also do not include any grain size (Hall-Petch) effects but these are typically small in the BCC HEAs, where as-cast alloy grain sizes are 80 - 200 μm which, using a rule-of-mixtures H-P parameter obtained from data on the refractory elements [29], leads to a strength increase of in the range of 27 - 43 MPa that is negligible. Ductility tests require larger, homogenized specimens with controlled low interstitial content, but the VEC= 4.75 is in the range needed for ductile alloys. These results further validate our design process for many of the key application requirements.

5. Discussion and summary

Nearly all the attractive quinary alloys have the minimum imposed 5% Ta content. Ta can be replaced by Nb, leading to quarternary Hf-Mo-Nb-Ti alloys that retain many properties while reducing the density and also facilitating processing. Equiatomic HfMoNbTi was very recently fabricated [28] and, as we predict, is single-phase as-cast, with room temperature strength of 1.28 GPa (1.66 GPa predicted) and VEC = 4.75. It shows low compression ductility, possibly due to the as-cast microstructure and/or interstitial content, but with smooth gradual failure without fracture (dark blue line in Fig. 2). Moving away from the equiatomic composition and applying the same performance criteria as for the 5-component alloys, we identify 15 new promising quarternary alloys (see Table B.3), all with lower density, higher specific strength, and comparable melting temperatures and phase separation temperatures to our attractive quinary alloys. In particular, the alloy $Hf_{15}Mo_{20}Nb_{25}Ti_{40}$ is predicted to have a strength at 1200 °C of 0.29 GPa, VEC = 4.65, melting point of 2054 °C, and density of only 8.19 g/cm^3, all except strength showing improvements over HfMoNbTi. This group of quarternary alloys is thus identified as a very promising domain for multi-performant high-temperature alloys.

To summarize, we have introduced a theory-guided alloy design process to discover new single-phase BCC refractory High Entropy Alloys possessing the suite of mechanical and thermodynamic properties needed for applications. The design process is parameter free and can be efficiently applied to alloys of any composition and number of components. Starting from a broad scope Cr-Hf-Mo-Nb-Ta-Ti-W-Zr alloys, we have discovered attractive quinary alloys in the Hf-Mo-Nb-Ta-Ti family that satisfy important performance requirements. One of these alloys, $Hf_{15}Mo_{25}Nb_{20}Ta_5Ti_{35}$, has been fabricated and tested for a number of properties, validating the methodology. A further selection of quarternary Hf-Mo-Nb-Ti alloys has also been identified as very promising for future study. Overall, this theory-guided design process is easily extend-

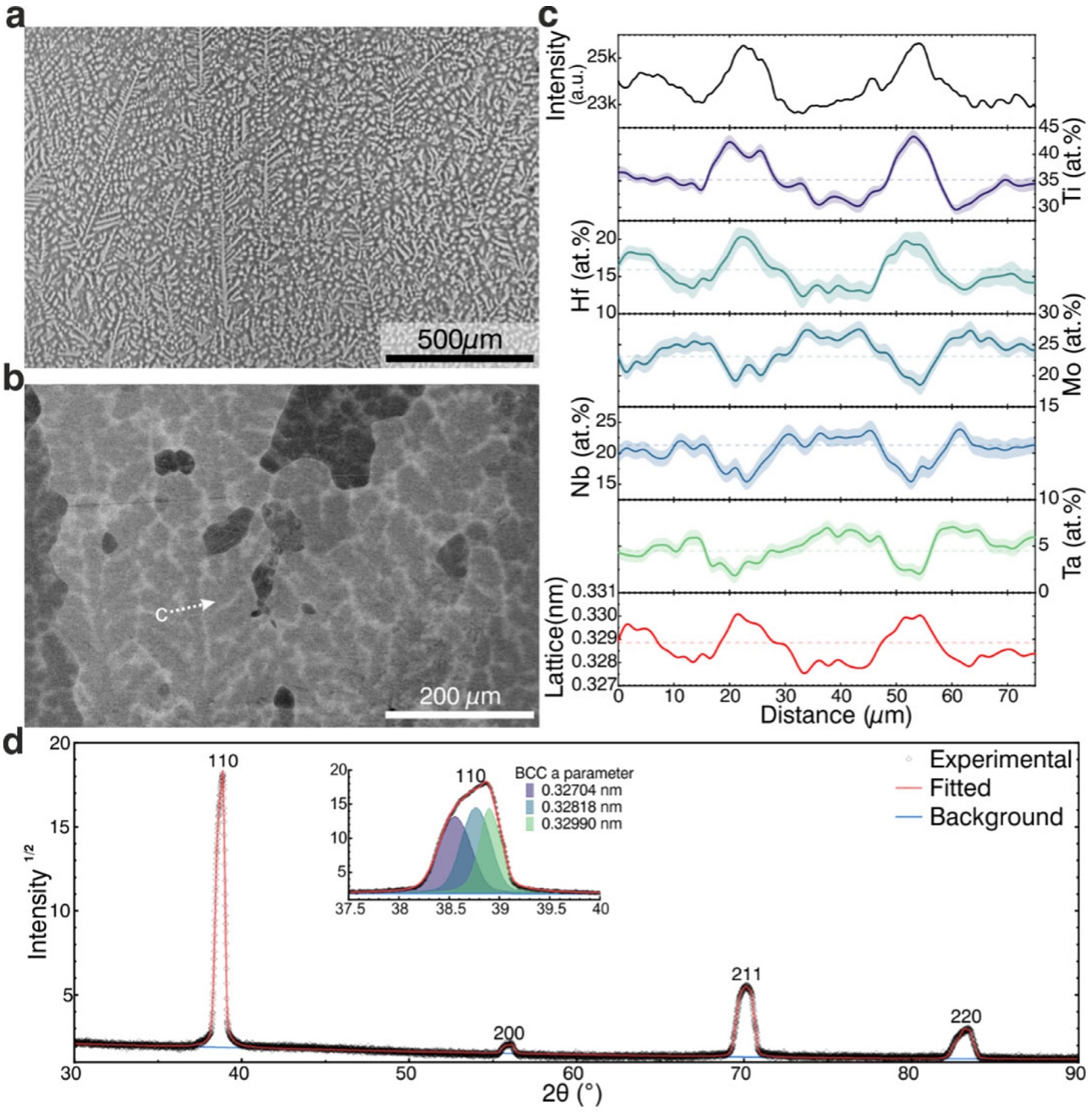

Fig. 4. Microstructural investigation of the arc-melted $Hf_{15}Mo_{25}Nb_{20}Ta_5Ti_{35}$ alloy. The alloy's microstructure is clearly dendritic, as revealed by a slight etching effect from the colloidal silica (a) or the chemical contrast by BSE-SEM (b). (c) Concentration profile (EDS) measured through the dendritic structure (indicated by the dashed arrow in (b)) allows to identify the segregation of Ti and Hf to the interdendritic domains, and Mo, Nb and Ti to the dendritic core regions. The dashed lines represent the average composition of the alloy. Using Vegard's law, a lattice parameter profile is calculated. (d) The XRD pattern only shows four peaks that correspond to a BCC structure. The peak shape asymmetry is due to pronounced effects due to elemental segregation, which leads to a variation of the lattice parameter by ~ 5%. Note: the peak height is affected by the material's texture.

able and so provides a reliable and efficient path for the discovery of next-generation high-temperature alloys.

Declaration of Competing Interest

The authors declare that they have no known competing financial interests or personal relationships that could have appeared to influence the work reported in this paper.

Acknowledgements

The authors gratefully acknowledge financial support from the Swiss National Science Foundation through both the NCCR MARVEL and project 20 0 021 18198/1 entitled "Harnessing atomic-scale randomness: design and optimization of mechanical performance in High Entropy Alloys". The authors would also like to acknowledge Irene Ferretto and Marvin Schuster (Empa) for their technical support during the XRD and SEM acquisitions, respectively.

Appendix A. Predicted thermodynamic properties of other alloys

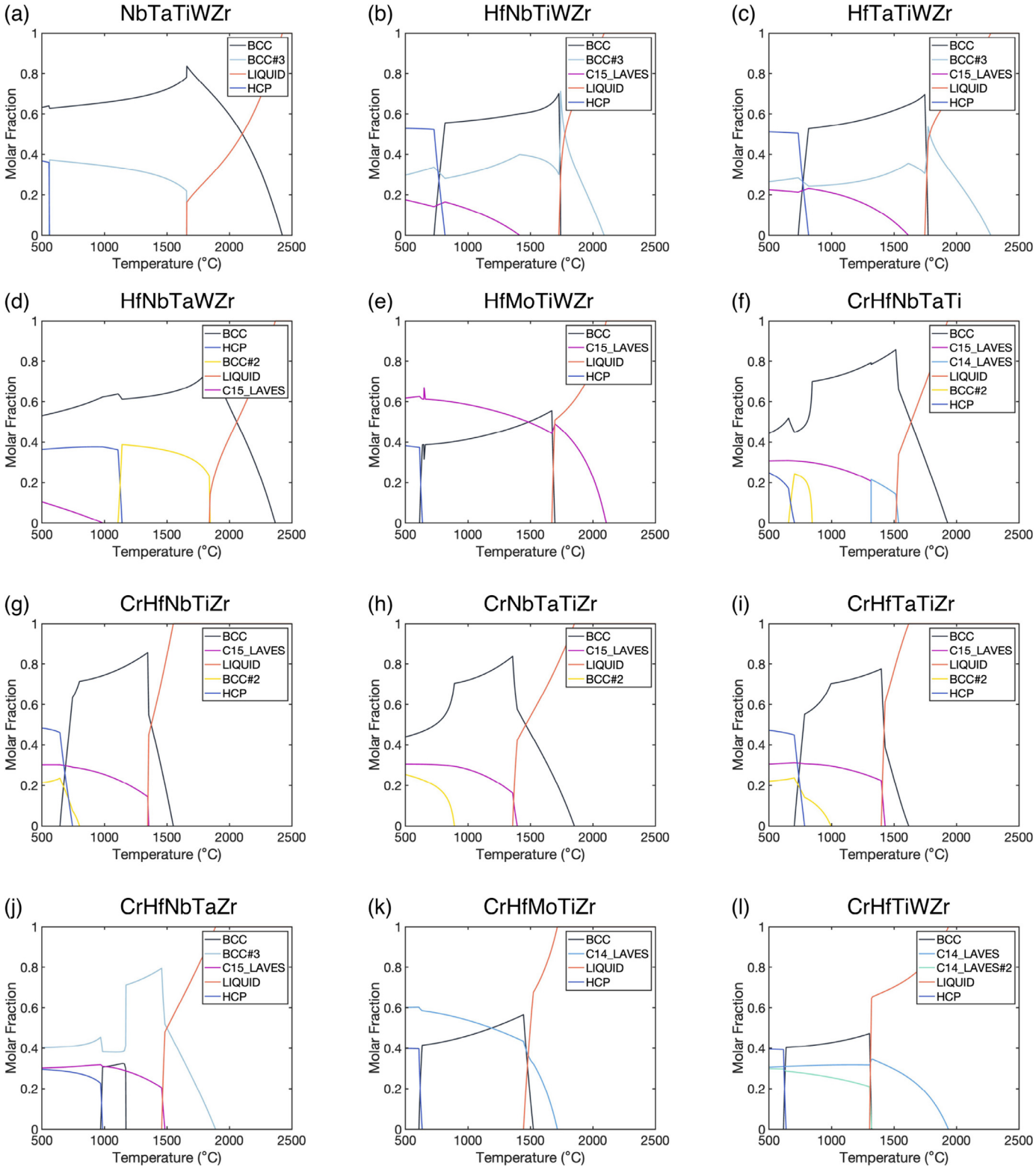

Fig. A.1. Molar fraction of stable phases as a function of temperature for the quinary alloys in the first group. The notations of BCC, BCC#2 and BCC#3 all represent BCC random solid solutions while HCP is a random HCP phase, C14_ LAVES and C15_ LAVES are C14 and C15 Laves phase structures, respectively.

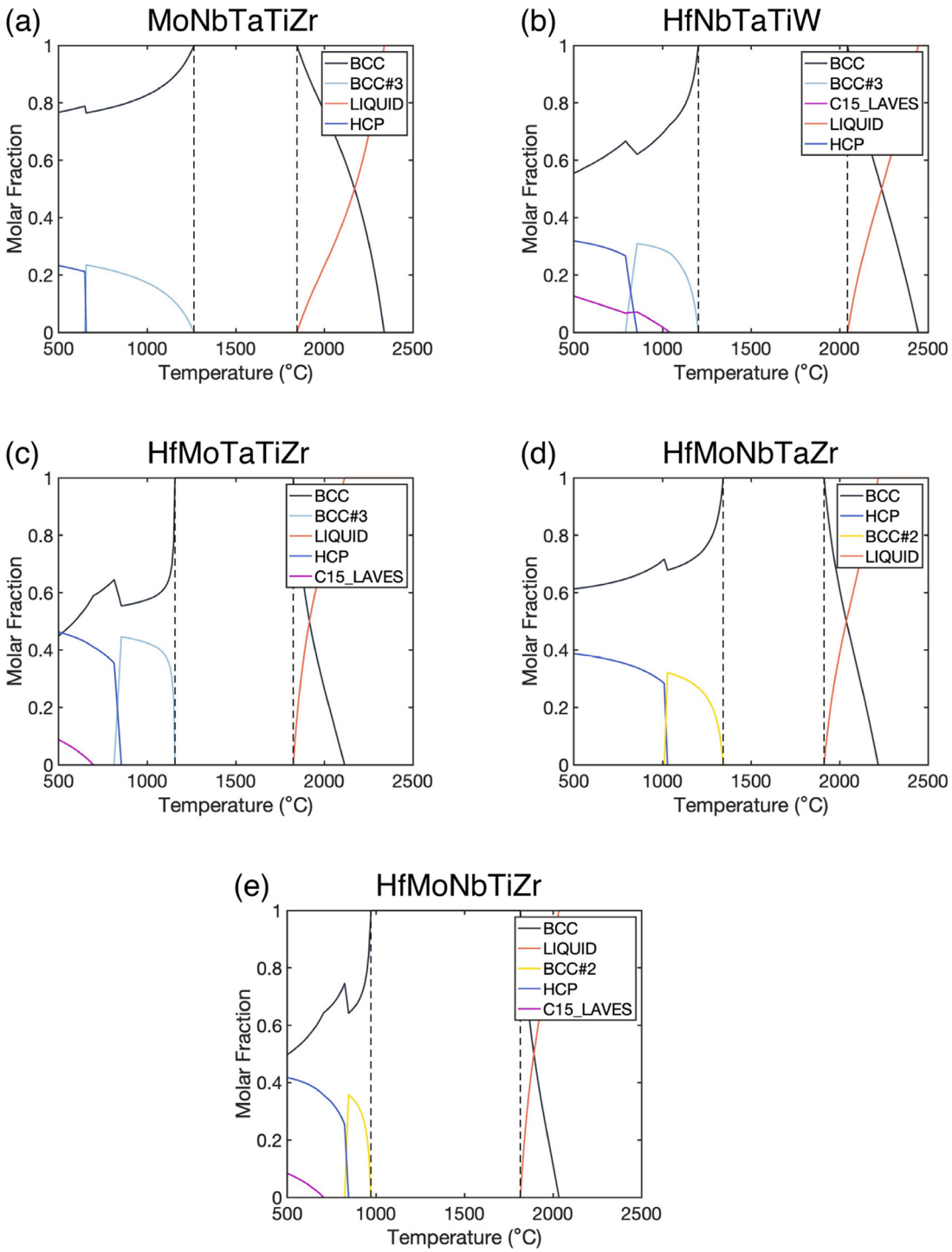

Fig. A.2. Molar fraction of stable phases as a function of temperature for the quinary alloys in the second group. The Thermocalc software notations of BCC, BCC#2 and BCC#3 all represent BCC random solid solutions while HCP is a random HCP phase, C14_ LAVES and C15_ LAVES are C14 and C15 Laves phase structures, respectively.

Appendix B. Detailed data of the studied alloys

Table B1
Key properties of the 6 selected equiatomic quinary alloys. ρ (g/cm^3) is the density, τ_y (GPa) is the predicted uniaxial tensile yield stress at room temperature, τ_y^* (GPa) is the predicted stress at 1200 °C, τ_y/ρ (kN · m/kg) is the specific strength, VEC is the valence electron count, T^* (°C) is the phase decomposition temperature and T_m (°C) is the melting temperature.

Alloy	τ_y	τ_y^*	ρ	VEC	τ_y/ρ	^{T*}	T_m
HfMoNbTaTi	1.48	0.48	10.84	4.80	136.40	854	2145
HfMoNbTiZr	1.66	0.55	8.73	4.60	189.86	971	1815
HfNbTaTiW	1.57	0.54	12.40	4.80	126.24	1202	2045
MoNbTaTiZr	1.60	0.55	9.20	4.80	173.81	1264	1846
HfMoTaTiZr	1.79	0.64	10.24	4.60	174.48	1157	1825
HfMoNbTaZr	1.90	0.73	10.95	4.80	173.35	1343	1912

Table B2
Key properties of the 10 selected off-equiatomic alloys together with those of HfMoNbTaTi for comparison. ρ (g/cm^3) is the density, τ_y (GPa) is the predicted uniaxial tensile yield stress at room temperature, τ_y^* (GPa) is the predicted stress at 1200 °C, τ_y/ρ (kN · m/kg) is the specific strength, VEC is the valence electron count, TT^* (°C) is the phase decomposition temperature and T_m (°C) is the melting temperature.

Alloy	τ_y	τ_y^*	ρ	VEC	τ_y/ρ	T^*	T_m
$Hf_{20}Mo_{20}Nb_{20}Ta_{20}Ti_{20}$	1.48	0.48	10.84	4.80	136.40	854	2145
$Hf_{10}Mo_{25}Nb_{15}Ta_{10}Ti_{40}$	1.12	0.30	8.79	4.75	127.60	560	2158
$Hf_{20}Mo_{15}Nb_{25}Ta_5Ti_{35}$	1.14	0.29	8.99	4.60	127.05	824	2015
$Hf_{15}Mo_{20}Nb_{20}Ta_5Ti_{40}$	1.15	0.30	8.59	4.65	134.17	705	2054
$Hf_{15}Mo_{20}Nb_{15}Ta_{10}Ti_{40}$	1.18	0.31	9.00	4.65	130.87	697	2054
$Hf_{15}Mo_{20}Nb_{25}Ta_5Ti_{35}$	1.18	0.31	8.79	4.70	134.09	732	2101
$Hf_{15}Mo_{20}Nb_{30}Ta_5Ti_{30}$	1.20	0.33	8.98	4.75	133.88	756	2139
$Hf_{15}Mo_{25}Nb_{15}Ta_5Ti_{40}$	1.32	0.38	8.67	4.70	152.14	642	2050
$Hf_{15}Mo_{25}Nb_{20}Ta_5Ti_{35}$	1.35	0.40	8.86	4.75	151.92	654	2103
$Hf_{15}Mo_{30}Nb_{10}Ta_5Ti_{40}$	1.49	0.47	8.74	4.75	169.93	816	2031
$Hf_{15}Mo_{35}Nb_5Ta_5Ti_{40}$	1.65	0.57	8.81	4.80	187.43	940	2004

Table B3
Key properties of the 15 selected off-equiatomic alloys together with those of HfMoNbTi for comparison. ρ (g/cm^3) is the density, τ_y (GPa) is the predicted uniaxial tensile yield stress at room temperature, τ_y^* (GPa) is the predicted stress at 1200 °C, τ_y/ρ (kN · m/kg) is the specific strength, VEC is the valence electron count,T^* (°C) is the phase decomposition temperature and T_m (°C) is the melting temperature.

Alloy	τ_y	τ_y^*	ρ	VEC	τ_y/ρ	T^*	T_m
$Hf_{25}Mo_{25}Nb_{25}Ti_{25}$	1.66	0.56	9.46	4.75	176.10	812	2028
$Hf_{20}Mo_{15}Nb_{30}Ti_{35}$	1.11	0.27	8.60	4.60	129.71	831	2011
$Hf_{15}Mo_{20}Nb_{25}Ti_{40}$	1.13	0.29	8.19	4.65	137.70	710	2054
$Hf_{20}Mo_{15}Nb_{35}Ti_{30}$	1.14	0.29	8.79	4.65	129.56	855	2045
$Hf_{15}Mo_{20}Nb_{30}Ti_{35}$	1.15	0.30	8.38	4.70	137.45	735	2098
$Hf_{20}Mo_{15}Nb_{40}Ti_{25}$	1.16	0.30	8.98	4.70	129.27	880	2073
$Hf_{15}Mo_{20}Nb_{35}Ti_{30}$	1.18	0.31	8.58	4.75	137.08	757	2132
$Hf_{15}Mo_{25}Nb_{20}Ti_{40}$	1.29	0.37	8.26	4.70	156.48	647	2052
$Hf_{20}Mo_{20}Nb_{25}Ti_{35}$	1.30	0.36	8.67	4.65	149.67	781	2022
$Hf_{15}Mo_{25}Nb_{25}Ti_{35}$	1.32	0.38	8.45	4.75	156.07	658	2102
$Hf_{20}Mo_{20}Nb_{30}Ti_{30}$	1.32	0.38	8.86	4.70	149.35	812	2059
$Hf_{15}Mo_{25}Nb_{30}Ti_{30}$	1.35	0.40	8.65	4.80	155.56	688	2140
$Hf_{15}Mo_{30}Nb_{15}Ti_{40}$	1.46	0.46	8.33	4.75	175.10	829	2035
$Hf_{20}Mo_{25}Nb_{20}Ti_{35}$	1.48	0.46	8.74	4.70	169.74	698	2019
$Hf_{20}Mo_{25}Nb_{25}Ti_{30}$	1.51	0.48	8.93	4.75	169.23	739	2060
$Hf_{20}Mo_{30}Nb_{15}Ti_{35}$	1.67	0.57	8.81	4.75	189.76	866	2005

References

[1] J.-W. Yeh, S.-K. Chen, S.-J. Lin, J.-Y. Gan, T.-S. Chin, T.-T. Shun, C.-H. Tsau, S.-Y. Chang, Nanostructured high-entropy alloys with multiple principal elements: novel alloy design concepts and outcomes, Adv. Eng. Mater. 6 (5) (2004) 299–303.

[2] B. Cantor, I. Chang, P. Knight, A. Vincent, Microstructural development in equiatomic multicomponent alloys, Mater. Sci. Eng. A 375 (2004) 213–218.

[3] K. Kaufmann, K.S. Vecchio, Searching for high entropy alloys: a machine learning approach, Acta Mater. 198 (2020) 178–222.

[4] Z. Zhang, M. Li, K. Flores, R. Mishra, Machine learning formation enthalpies of intermetallics, J. Appl. Phys. 128 (10) (2020) 105103.

[5] D.P. Santos, P. Pelissari, R.F. de Mello, V.C. Pandolfelli, Estimating the thermal insulating performance of multi-component refractory ceramic systems based on a machine learning surrogate model framework, J. Appl. Phys. 127 (21) (2020) 215104.

[6] E. Mazhnik, A.R. Oganov, Application of machine learning methods for predicting new superhard materials, J. Appl. Phys. 128 (7) (2020) 075102.

[7] P.V. Balachandran, B. Kowalski, A. Sehirlioglu, T. Lookman, Experimental search for high-temperature ferroelectric perovskites guided by two-step machine learning, Nat. Commun. 9 (1) (2018) 1–9.

[8] P.V. Balachandran, Machine learning guided design of functional materials with targeted properties, Comput. Mater. Sci 164 (2019) 82–90.

[9] F. Maresca, W.A. Curtin, Mechanistic origin of high strength in refractory BCC high entropy alloys up to 1900k, Acta Mater. 182 (2020) 235–249.

[10] C. Lee, F. Maresca, R. Feng, Y. Chou, T. Ungar, M. Widom, K. An, J.D. Poplawsky, Y.-C. Chou, P.K. Liaw, et al., Strength can be controlled by edge dislocations in refractory high-entropy alloys, Nat. Commun. 12 (1) (2021) 1–8.

[11] F. Maresca, W.A. Curtin, Theory of screw dislocation strengthening in random BCC alloys from dilute to “high-entropy” alloys, Acta Mater. 182 (2020) 144–162.

[12] S.I. Rao, C. Woodward, B. Akdim, O.N. Senkov, D. Miracle, Theory of solid solution strengthening of BCC chemically complex alloys, Acta Mater. 209 (2021) 116758.

[13] R.O. Scattergood, D.J. Bacon, The Orowan mechanism in anisotropic crystals, Philos. Mag. 31 (1) (1975) 179–198.

[14] D.J. Bacon, D.M. Barnett, R.O. Scattergood, Anisotropic continuum theory of lattice defects, Prog. Mater. Sci. 23 (1980) 51–262.

[15] L. Kubin, Dislocations, Mesoscale Simulations and Plastic Flow, volume 5, Oxford University Press, 2013.

[16] X. Li, W. Li, D.L. Irving, L.K. Varga, L. Vitos, S. Schönecker, Ductile and brittle crack-tip response in equimolar refractory high-entropy alloys, Acta Mater. 189 (2020) 174–187.

[17] Y.-J. Hu, A. Sundar, S. Ogata, L. Qi, Screening of generalized stacking fault energies, surface energies and intrinsic ductile potency of refractory multicomponent alloys, Acta Mater. 210 (2021) 116800.

[18] E. Mak, B. Yin, W.A. Curtin, A ductility criterion for bcc high entropy alloys, J. Mech. Phys. Solids 152 (2021) 104389.

[19] C. Yang, L. Qi, Ab initio calculations of ideal strength and lattice instability in W-Ta and W-Re alloys, Phys. Rev. B 97 (1) (2018) 014107.

[20] F.G. Coury, T. Butler, K. Chaput, A. Saville, J. Copley, J. Foltz, P. Mason, K. Clarke, M. Kaufman, A. Clarke, Phase equilibria, mechanical properties and design of quaternary refractory high entropy alloys, Mater. Des. 155 (2018) 244–256.

[21] N. Yurchenko, N. Stepanov, G. Salishchev, Laves-phase formation criterion for high-entropy alloys, Mater. Sci. Technol. 33 (1) (2017) 17–22.

[22] S.Y. Chen, X. Yang, K.A. Dahmen, P.K. Liaw, Y. Zhang, Microstructures and crackling noise of AlxNbTiMoV high entropy alloys, Entropy 16 (2) (2014) 870–884.

[23] E.S. Panina, N.Y. Yurchenko, S.V. Zherebtsov, M.A. Tikhonovsky, M.V. Mishunin, N.D. Stepanov, Structures and mechanical properties of Ti-Nb-Cr-V-Ni-Al refractory high entropy alloys, Mater. Sci. Eng. A 786 (2020) 139409.

[24] H. Chen, A. Kauffmann, S. Laube, I.-C. Choi, R. Schwaiger, Y. Huang, K. Lichtenberg, F. Müller, B. Gorr, H.-J. Christ, et al., Contribution of lattice distortion to solid solution strengthening in a series of refractory high entropy alloys, Metall. Mater. Trans. A 49 (3) (2018) 772–781.

[25] J.H. DeVan, Catastrophic Oxidation of High-Temperature Alloys, Technical Report, Oak Ridge National Lab., Tenn., 1961.

[26] A. Mukherjee, S.P. Wach, Kinetics of the oxidation of vanadium in the temperature range 350–950 °C, J. Less Common Metals 92 (2) (1983) 289–300.

[27] K.-K. Tseng, C.-C. Juan, S. Tso, H.-C. Chen, C.-W. Tsai, J.-W. Yeh, Effects of Mo, Nb, Ta, Ti, and Zr on mechanical properties of equiatomic Hf-Mo-Nb-Ta-Ti-Zr alloys, Entropy 21 (1) (2019) 15.

[28] X. Yang, Z. An, Y. Zhai, X. Wang, Y. Chen, S. Mao, X. Han, Effect of Al content on the thermal oxidation behaviour of AlHfMoNbTi high-entropy alloys analysed by in situ environmental TEM, Corros Sci. 191 (2021) 109711.

[29] Z.C. Cordero, B.E. Knight, C.A. Schuh, Six decades of the Hall–Petch effect–a survey of grain-size strengthening studies on pure metals, Int. Mater. Rev. 61 (8) (2016) 495–512.